J Mater Sci (2011) 46:5378–5384
DOI 10.1007/s10853-011-5476-x

One-pot synthesis and photocatalytic activity of Fe-doped TiO_2 films with anatase–rutile nanojunction prepared by plasma electrolytic oxidation

Tetsuro Soejima · Hitomi Yagyu · Seishiro Ito

Received: 30 December 2010 / Accepted: 15 March 2011 / Published online: 29 March 2011

Abstract A novel one-pot low temperature preparation of Fe-doped anatase–rutile TiO_2 (Fe-TiO_2) films is demonstrated using plasma electrolytic oxidation (PEO). Pale yellow TiO_2 films are obtained by PEO treatment of Ti metals in the electrolyte dispersing TiO_2 and Fe_2O_3 particles. The oxidized layer on Ti metal have a sponge-like structure with thickness and pore size of 10 and 0.1–1 μm, respectively. Investigation by X-ray diffraction, X-ray photoelectron spectroscopy, and UV–Vis absorption spectroscopy all indicate that dissolved Fe^{3+} ions in the strong acidic electrolyte are doped into the TiO_2 structure during PEO. The photocatalytic activity of Fe-TiO_2 samples was investigated by studying the photocatalytic decomposition of acetaldehyde. Fe-TiO_2 samples doped with optimum Fe content show visible light photocatalytic activity and further increased photocatalytic activity under UV illumination compared with that of pure TiO_2 films.

Introduction

Titanium dioxide (TiO_2) has aroused great interest because of its high photocatalytic activity, chemical stability, low-toxicity, and low cost [1, 2]. The large band gap of TiO_2 (anatase, 3.2 eV) requires UV excitation which accounts for only a small portion (3–5%) of the solar spectrum. To enhance photocatalytic activity under sunlight conditions, more efficient utilization of the solar spectrum is essential. The spectral response of TiO_2 can be extended to the visible region by doping with transition metals [3–5]. Fe is considered an appropriate candidate as the ionic radius of Fe^{3+} (0.78 Å) is similar to that of Ti^{4+} (0.74 Å) [6]. Fe^{3+} ions are easily incorporated into the crystal structure of TiO_2. Replacing Ti^{4+} with Fe^{3+} in the TiO_2 lattice forms a localized band near the bottom of conduction band, thus decreasing the band gap. Fe^{3+} doping has also been reported to improve charge separation of generated excited electrons and holes in TiO_2 [11]. Most authors have suggested that Fe^{3+} ions act as trapping sites for excited electrons and/or holes, resulting in the decrease of charge carrier recombination. Fe-doped TiO_2 can be excited by visible light and its photocatalytic activity under UV illumination is also enhanced [7–13]. To date, various synthetic routes to Fe-doped TiO_2 materials have been reported, most of which are sol–gel [7–10] and hydrothermal techniques [11–13]. These methods generally require long reaction times, high temperatures, and multi-step process.

Plasma electrolytic oxidation (PEO) of metals has attracted much industrial and academic attention because functional metal oxide films such as TiO_2, Al_2O_3, MgO, and $BaTiO_3$ can be easily obtained [14–18]. The PEO process is an effective method to prepare transition metal-doped TiO_2 photocatalysts. Cr-doped TiO_2 films prepared by PEO process show excellent photocatalytic activity for degradation of methylene blue and decomposition of water under visible light illumination [19]. Yao et al. [20] prepared Zn-doped TiO_2 films and investigated the photocatalytic activity in the reduction of potassium chromate under UV light illumination. We have developed a synthetic pathway to a TiO_2 photocatalyst by PEO of Ti metal in binary or trinary electrolyte solutions [21]. The one-pot

T. Soejima · H. Yagyu · S. Ito
Department of Applied Chemistry, Kinki University, Higashiosaka, Japan

T. Soejima (✉)
CREST, Japan Science and Technology Agency, 3-4-1 Kowakae, Higashi-osaka, Osaka 577-8502, Japan
e-mail: soejima@apch.kindai.ac.jp

method is low temperatures process and is adaptable to large-scales. Resulting TiO_2 films are a composite of anatase and rutile phases. Such phase coupling greatly improves charge separation of excited electrons and holes [22], and anatase–rutile coupled TiO_2 materials have higher photocatalytic activity compared with that of TiO_2 with anatase or rutile single phase. The anatase/rutile TiO_2 film formed (A/R) by PEO also shows high photocatalytic activity under UV illumination. Incorporation of anatase TiO_2 nanoparticles into the A/R film can be achieved by dispersing anatase TiO_2 nanoparticles within the electrolyte solution, and the resulting A/A/R TiO_2 material showed further increased photocatalytic activity [21].

Herein, we report a one-pot synthetic method for preparing Fe-doped A/A/R TiO_2 (Fe-TiO_2) films by PEO of Ti metal at room temperature. Anatase TiO_2 and α-Fe_2O_3 particles are both dispersed in the electrolyte solution composed of hydrogen peroxide, phosphoric acid, and sulfuric acid. The Fe_2O_3 particles are partly dissolved in the strongly acidic electrolyte solution, and Fe ions are incorporated into the TiO_2 film during PEO. Resulting films show visible light photocatalytic activity for the decomposition of acetaldehyde. Recently, Wu et al. [23] reported that TiO_2 films prepared with Fe^{3+} addition electrolyte of H_2SO_4 using micro-plasma oxidation showed higher photocatalytic activities than that prepared in the pure electrolyte. However, their and most other studies for Fe-doped TiO_2 photocatalyst have discussed the photocatalytic activity under UV or visible light illumination. We investigated the photocatalytic activity of Fe-TiO_2 under UV, visible, and UV–Vis light irradiation to reveal the effect of Fe^{3+} doping to TiO_2 photocatalyst in detail.

Experimental section

Preparation of Fe-doped A/A/R TiO_2 film by plasma electrolytic oxidation

A Ti plate (purity, 99.9%; working area, 15 cm^2) was anodized galvanostatically at 3.0 A dm^{-2} for 1 h by using a regulated DC power supply. An aqueous electrolyte was prepared from a solution of sulfuric acid (1.50 M), hydrogen peroxide (0.30 M), and phosphoric acid (0.03 M). Anatase TiO_2 (20 g L^{-1}; mean diameter, 30 nm; TAYCA, AMT-600) and α-Fe_2O_3 particles (0–7 g L^{-1}; mean diameter, 300 nm; Kanto Chemical) were added to the electrolyte. The initial electrolyte temperature was 5 °C, and then the temperature was gradually increased to ca. 30 °C during PEO process. PEO treatment was carried out in a double-walled glass cell with continuous stirring. A Ti sheet was used as the cathode. After oxidation, the samples were washed with distilled water and dried at room temperature. It was confirmed that the dispersed Fe_2O_3 particles were partly dissolved (ca. 2 wt%) in the electrolyte by inductively coupled plasma-atomic emission spectrometry (ICP-AES) measurement.

Characterization

Field-emission scanning electron microscopy (SEM) and scanning electron microscopy/energy dispersive X-ray analysis (SEM/EDX) were performed using Hitachi S-4800 type II (accelerating voltage, 10 kV). X-ray diffraction (XRD) was performed using Rigaku RINT 2500 using Cu Kα radiation. UV–Vis diffuse reflectance spectra were obtained on Hitachi U-4000 spectrophotometer. X-ray photoelectron spectroscopy (XPS) was performed using AXIS-NOVA, KRATOS. For XPS measurement, powder samples were obtained by scratching the surface of obtained Fe-TiO_2 films, and the powder adhered to double-faced conductive carbon tape on sample stage for XPS. The measured binding energies were referenced to the C 1s line at 284.6 eV. ICP-AES was performed using Shimadzu ICPS-7500.

Photocatalytic experiments

The photocatalytic activities of sample films were evaluated by measuring the change in concentration of acetaldehyde. A closed Pyrex glass ($\lambda > 300$ nm) was used as the photo-reactor vessel with a volume of 640 cm^3. The sample film (30 × 30 mm^2) was placed in the reaction vessel. Two hundred ppm of acetaldehyde was prepared in the vessel by injection of a commercial acetaldehyde gas (Takachiho Chemical Industrial Co. Ltd.; 594 ppm; balance gas, N_2). The photo-irradiations were conducted at room temperature after equilibrium between the gaseous and adsorbed acetaldehyde had been reached (as ascertained by monitoring the concentration chromatographically about every 15 min). A 500-W Xe lamp (Wacom Electric, HX-500) was used as a light source. Three types of light beam, (i) UV light shorter than 400 nm, $I_{320–380} = 2.0$ mW cm^{-2}; (ii) visible light longer than 420 nm, $I_{400–485} = 2.0$ mW cm^{-2}; (iii) UV/visible light, $I_{320–380} = 2.0$ mW cm^{-2}, were irradiated to the samples by using cut filters (AGC Techno glass, UV-D36A; Toshiba, L-42). The decrease in acetaldehyde concentration during photoirradiation was measured using a gas chromatograph (Shimadzu, GC-2014, FID detector).

Results and discussion

Figure 1a shows photographic images of a Ti plate before and after PEO. A colorless A/A/R TiO_2 film was uniformly

formed on Ti plate in the absence of Fe_2O_3 in the electrolyte (Fig. 1a; right, A/A/R TiO_2). A pale yellow film was obtained by anodizing a Ti plate in electrolyte containing Fe_2O_3 (Fig. 1a; right, Fe-TiO_2). SEM images of a typical sample are shown in Fig. 1b, c. The oxidized layer had a sponge-like structure with thickness and pore size of 10 and 0.1–1 μm, respectively. Nano-sized particles were apparent on the Fe-TiO_2 surface, and anatase nanoparticles were expected to be deposited during PEO [21].

The crystalline structure was investigated from XRD patterns (Fig. 2). Diffractions from Ti and anatase and rutile TiO_2 were observed in the XRD spectra of all samples (JCPDS no. anatase, 21-1272; rutile, 21-1276; Ti, 44-1294). This was in contrast to diffractions of Fe_2O_3. Fe contents of prepared Fe-TiO_2 films were determined by ICP-AES measurement (Fig. 3). Fe content increased with dispersed Fe_2O_3 particle content (x g L^{-1}). Fe ions dispersed in the electrolyte were expected to be incorporated into the TiO_2 film crystal lattice. However, for Fe-TiO_2 samples, large particles (diameter, 100–300 nm) which are different from TiO_2 nanoparticles (diameter, 30 nm) were slightly seen on the surface of formed TiO_2 films as indicated by arrows on Fig. 4b, c. Figure 5 shows a SEM image and SEM/EDX elemental mappings of the Fe-TiO_2 film (x, 7 g L^{-1}). The signals attributed with Ti and O were evenly seen on the images. On the other hand, regions where large particles exist were particularly rich in elemental Fe. Thus, the large particles were probably Fe_2O_3 particles deposited on the surface of TiO_2 during PEO process. It is assumed that XRD signals attributed with Fe_2O_3 was not able to detect because of the negligible amount of the deposited Fe_2O_3 particles. The changes of cell volume and lattice parameters (a, b, and c) of anatase TiO_2 were not seen on the obtained Fe-TiO_2 samples [23]. Anatase TiO_2 nanoparticles dispersed in the electrolyte will be deposited into Fe-TiO_2 films during PEO process [21]. XRD signals attributed to anatase crystal doped with Fe^{3+} ions are hidden due to those of the deposited anatase nanoparticles. Thus, slight changes of the diffraction angle should not emerge on Fe-TiO_2 samples. Interestingly, the anatase:rutile diffraction intensity ratio changed by varying the Fe_2O_3 content in the electrolyte. This crystalline transformation was associated with local exothermic heat caused by the spark discharge process. Anatase:rutile ratio changes have also been reported for the PEO preparation of TiO_2 films from Ti plate in electrolytes containing Ni ions [24].

Figure 6 shows UV–Vis diffuse reflectance spectra for the obtained samples. All samples showed an intense broad

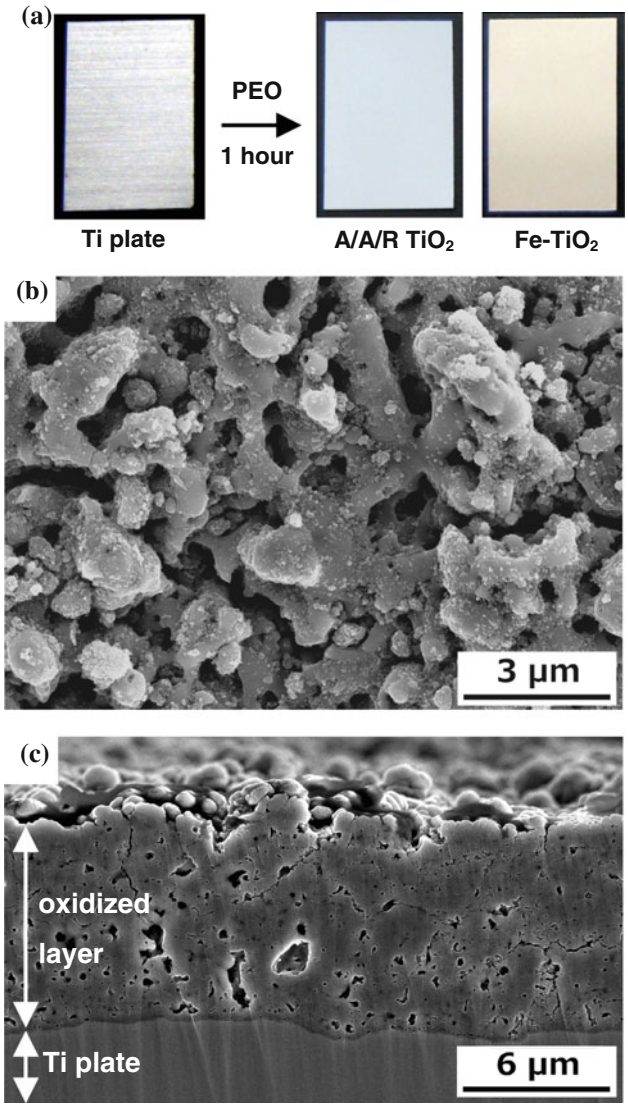

Fig. 1 **a** Photographic images of a Ti plate before (*left*) and after (*right*) PEO. **b** Plane and **c** cross-sectional scanning electron microscopy images of a Fe-TiO_2 film formed from PEO. The electrolyte dispersion contained 3 g of Fe_2O_3

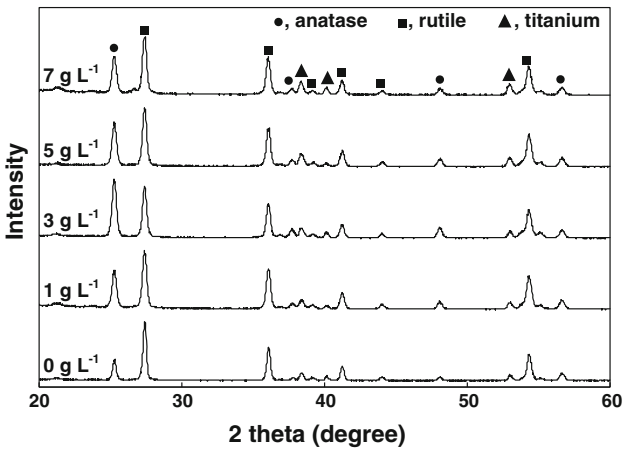

Fig. 2 XRD patterns of Fe-TiO_2 films obtained from PEO. Electrolyte dispersions contained various amounts of Fe_2O_3 (x g L^{-1}) as stated

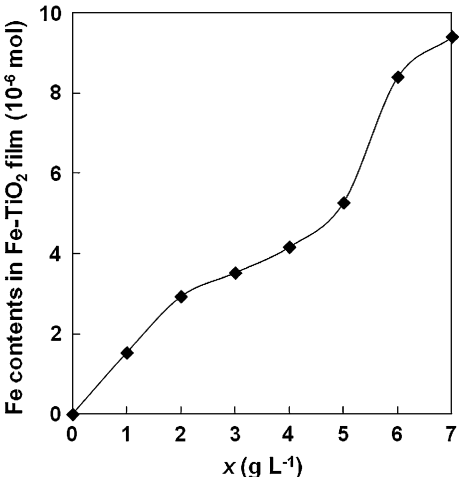

Fig. 3 Fe contents of Fe-TiO_2 samples prepared by the PEO process. Electrolyte dispersions contained various amounts of Fe_2O_3 (x g L^{-1}) as stated

absorption band below 400 nm which was attributed to the TiO_2 band-gap transition. The absorption bands in the visible and near infrared (NIR) region of the A/A/R TiO_2 film (0 g L^{-1}) were attributed with d−d transition of Ti^{3+} species which were slightly formed in the TiO_2 lattice by the plasma electrolytic oxidation process [21, 25]. For Fe-TiO_2 samples, an absorption bands emerged in visible, extending to the NIR region (400−750 nm), and its intensity increased with dispersed Fe_2O_3 content. Visible absorption (400–500 nm) may have been attributed to the excitation of Fe^{3+} 3d electrons to the TiO_2 conduction band at 415 nm or charge transfer transition between Fe ions (such as $Fe^{3+} + Fe^{3+} \rightarrow Fe^{4+} + Fe^{2+}$) at 500 nm [7]. The increases of absorption intensity in the Vis–NIR region (500–750 nm) have been usually observed on Fe-doped TiO_2 samples prepared by other procedures such as metal plasma ion implantation [26], sol–gel [27], hydrothermal [28], ultrasonic-hydrothermal [29], and incipient wetness impregnation methods [30]. The absorption bands are generally associated with one type of transitions, i.e., the promotion of an electron from a localized orbital on one atom to a higher-energy localized orbital on the same atom [31]. In this study, the absorption was associated with d−d electron transition of doped iron atoms and slightly deposited Fe_2O_3 particles.

XPS spectra of Fe-TiO_2 samples are shown in Fig. 7. Ti $2p_{1/2}$ and Ti $2p_{3/2}$ spin-orbital splittings were located at 464.4 and 458.7 eV, respectively, and were in agreement with literature values of Ti^{4+} in pure TiO_2 (Fig. 7a) [32]. These energies were not affected by the low doping content. Peaks attributed to Ti^{3+} were not observed in XPS spectra because of the very low contents in the TiO_2 crystal lattice. Peaks at 711.4–712.7 and 725.2–726.6 eV were assigned to Fe $2p_{3/2}$ and Fe $2p_{1/2}$, respectively

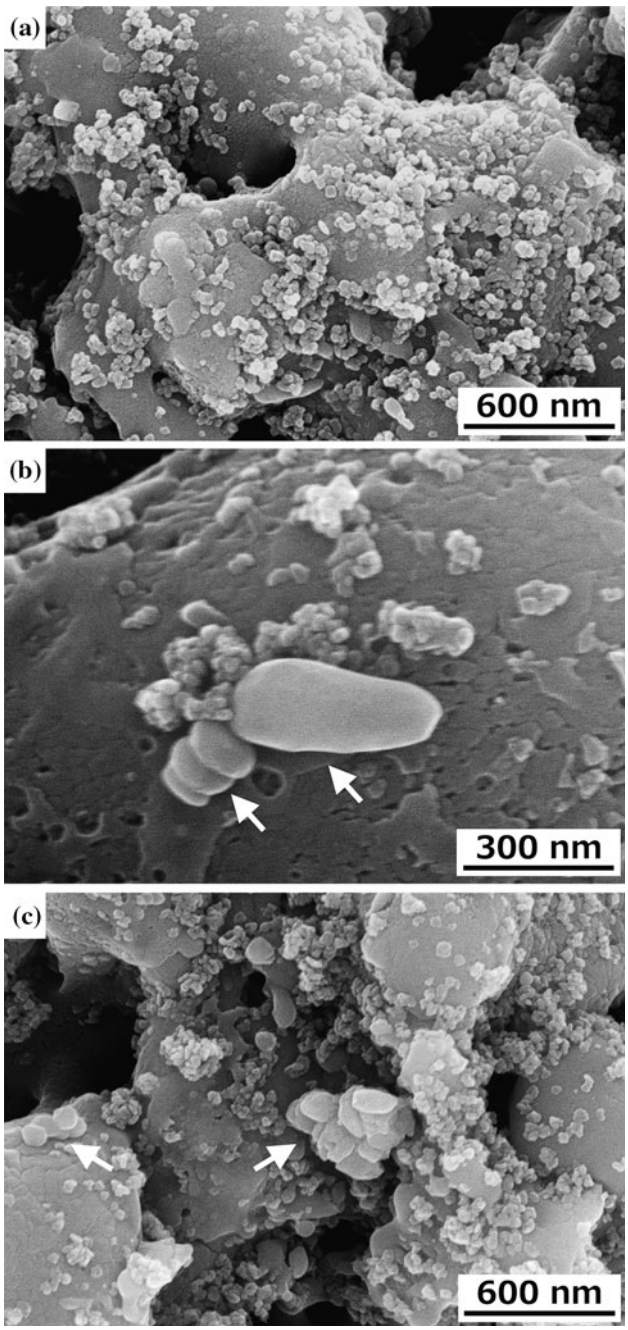

Fig. 4 SEM images of A/A/R TiO_2 film (**a**) and Fe-TiO_2 films obtained in electrolytes containing 3 g L^{-1} (**b**) and 7 g L^{-1} (**c**) Fe_2O_3 particles

(Fig. 7b). These signals showed a positive shift compared to those for crystalline α-Fe_2O_3 (711.0 and 724.4 eV for $2p_{3/2}$ and $2p_{1/2}$, respectively [33, 34]). Such positive shifts have been previously shown for Fe^{3+}-doped TiO_2 materials [7, 13]. Slight shifts in Fe 2p binding energy probably indicated some Fe^{3+} replaced Ti^{4+} within the TiO_2 lattice, and subsequent electron transfer from Fe^{3+} to Ti^{4+}. XRD, UV–Vis absorption, and XPS spectral data all

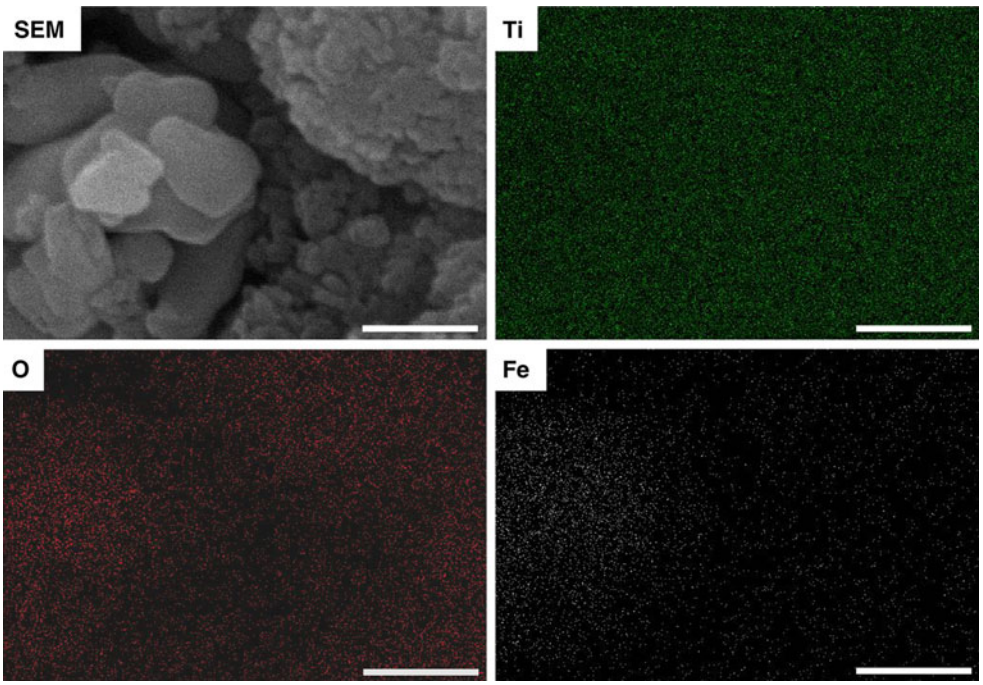

Fig. 5 SEM/EDX micrographs of Fe-TiO_2 (x, 7 g L^{-1}), with elemental analysis maps of Ti (*top right*), O (*bottom left*), and Fe (*bottom right*). *Scale bar* 200 nm

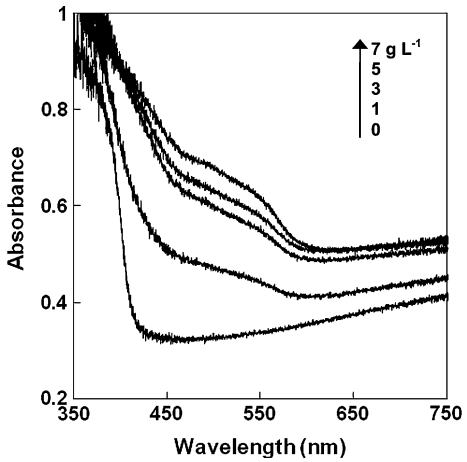

Fig. 6 UV–Vis diffuse reflectance spectra of Fe-TiO_2 films. Electrolyte dispersions contained various amounts of Fe_2O_3 (x g L^{-1}) as stated

indicated that dissolved Fe^{3+} was doped into the TiO_2 structure during PEO.

The photocatalytic activity of Fe-TiO_2 samples was investigated by studying the photocatalytic decomposition of acetaldehyde under UV, visible, and UV–vis illumination. Photocatalytic degradation kinetics of organic compounds usually follows the Langmuir–Hinshelwood mechanism [35, 36], simplified to the apparent first-order equation:

$$\ln\left(\frac{C_0}{C}\right) = kKt = k_{app}t$$

where C_0 and C are the concentration of acetaldehyde initially and after t min, respectively, k is the reaction rate constant, and K is the adsorption coefficient of the reactant. The apparent first-order rate constant, k_{app} is given by the gradient of the graph of $\ln(C_0/C)$ versus t.

Figure 8 shows k_{app} values of Fe-TiO_2 samples obtained from varying amounts of Fe_2O_3 (x) dispersed in the electrolyte. The A/A/R TiO_2 (x, 0 g L^{-1}) film showed photocatalytic activity under UV illumination. On the other hand, Fe-TiO_2 samples ($1 < x < 6$) clearly showed visible light photocatalytic activity. Figure 9 shows the changes in $\ln(C_0/C)$ values of the Fe-TiO_2 (x, 3 g L^{-1}) and the A/A/R TiO_2 (x, 0 g L^{-1}) under visible light irradiation. The negligible photocatalytic activity of the A/A/R TiO_2 film was attributed with the self-doped Ti^{3+} species [37]. On the other hand, the visible light photocatalytic activity of the Fe-TiO_2 film was about ten times as high as that of the A/A/R TiO_2 film. Fe^{3+} 3d electrons can be excited by the visible light and transit to the conduction band of TiO_2. The photocatalytic activities were investigated in gas phase containing air, N_2, and acetaldehyde. H_2O and O_2 molecules from air were present in the reaction vessel. Additionally, H_2O molecules are generated as products of photocatalytic oxidation of acetaldehyde [38]. The photogenerated holes and electrons are reacted with H_2O and O_2 on the surface of Fe-TiO_2, resulting in the formation of highly activated radicals, such as O_2^- and HO. Acetaldehyde molecules adsorbed on the surface of the

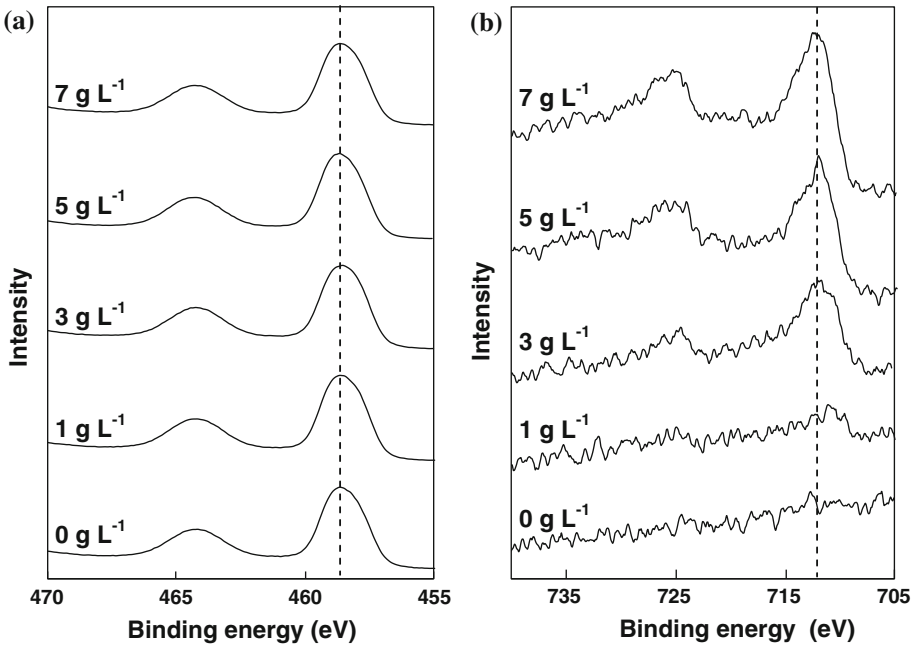

Fig. 7 Ti 2p (**a**) and Fe 2p (**b**) XPS spectra of Fe-TiO_2 samples obtained by the PEO process. Electrolyte dispersions contained various amounts of Fe_2O_3 (x g L^{-1}) as stated

photocatalyst are oxidatively decomposed by the formed radicals. In addition, the slightly deposited Fe_2O_3 particles onto the surfaces of TiO_2 were involved in the increase of visible light photocatalytic activity [39]. The photocatalytic decomposition of acetaldehyde occurs on also pure TiO_2 by generating holes and excited electrons with UV light illumination. For Fe-TiO_2 samples under excitation, k_{app} initially increased with dispersed Fe_2O_3 content, and then plateaued at 3 g L^{-1} of Fe_2O_3. Further Fe_2O_3 increase caused a decrease in photocatalytic activity. A small amount of doped Fe^{3+} can act as trapping sites for holes and excited electrons, respectively, generated in the valence band and the conduction band of TiO_2 under UV illumination and reduce the recombination probability [11]. Thus, photocatalytic activities of Fe-TiO_2 ($1 < x < 3$) were enhanced under UV light excitation compared with that of pure TiO_2. This enhancement was probably associated with the increased anatase:rutile ratio. Anatase TiO_2 photocatalysts show higher photocatalytic activity compared with that of rutile TiO_2 [40]. All the above photocatalytic reaction pathways are involved in the photocatalytic activity of Fe-TiO_2 under visible and UV light illumination (Fig. 8). In addition, the interaction between Fe-TiO_2 and acetaldehyde which was changed due to the formation of surface Fe–OH sites perhaps influenced the photocatalytic activity. However, doped Fe^{3+} may also act as recombination centers for photo-generated holes and electrons when their concentration is higher than the optimal level [41–43]. Thus, photocatalytic activity under both visible and UV illumination decreased due to less photo-generated carriers when the doped Fe content exceeded a certain concentration ($4 < x < 7$).

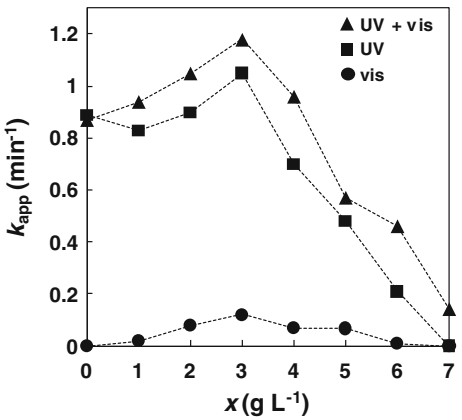

Fig. 8 First-order rate constants (k_{app}) for the photocatalytic degradation of acetaldehyde by Fe-TiO_2 films under UV–Vis (*filled triangle*), UV (*filled square*), and visible (*filled circle*) light excitation, as a function of electrolyte Fe_2O_3 content (x g L^{-1})

Conclusions

In conclusion, porous Fe-doped TiO_2 films containing both anatase and rutile crystal phases were obtained by a one-pot PEO process. The Fe-TiO_2 samples possessed an absorption band in the visible region and showed visible light photocatalytic activity for the decomposition of acetaldehyde. In addition, the photocatalytic activities of Fe-TiO_2 samples were enhanced under also UV illumination due to the decrease of recombination probability of photo-generated holes and electrons by formation of trapping sites attributed to incorporation of Fe^{3+} ions into TiO_2 crystal lattice. We envisage that metal-doped TiO_2 materials of various compositions can be obtained from PEO.

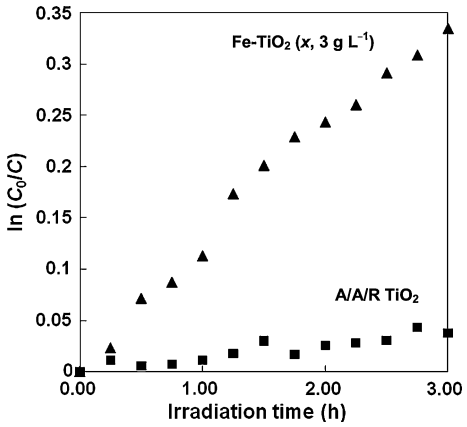

Fig. 9 Kinetics of the photocatalytic degradation of acetaldehyde by Fe-TiO_2 (*filled triangle*) and A/A/R TiO_2 (*filled square*) under visible light irradiation, as a function of irradiation time

Acknowledgement This study was financially supported by a Grant-in-Aid for Young Scientists (B, no. 22710102) from the Ministry of Education, Culture, Sports, Science and Technology, Japan and JST CREST.

References

1. Linsebigler AL, Lu G, Yates JT (1995) Chem Rev 95:735
2. Tachikawa T, Fujitsuka M, Majima T (2007) J Phys Chem C 111:5259
3. Di Paola A, Marcì G, Palmisano L, Schiavello M, Uosaki K, Ikeda S, Ohtani B (2002) J Phys Chem B 106:637
4. Anpo M, Takeuchi M (2003) J Catal 216:505
5. Chen X, Mao SS (2007) Chem Rev 107:2891
6. Lide DR (ed) (2004) CRC handbook of chemistry and physics, 85th edn. CRC Press, Boca Raton
7. Zhu J, Chen F, Zhang J, Chen H, Anpo M (2006) J Photochem Photobiol A 180:196
8. Egerton TA, Kosa SAM, Christensen PA (2006) Phys Chem Chem Phys 8:398
9. Vijayan P, Mahendiran C, Suresh C, Shanthi K (2009) Catal Today 141:220
10. Choi J, Park H, Hoffman MR (2010) J Phys Chem C 114:783
11. Zhu J, Zheng W, He B, Zhang J, Anpo M (2004) J Mol Catal A 216:35
12. Nunes MR, Monteiro OC, Castro AL, Vasconcelos DA, Silvestre AJ (2008) Euro J Inorg Chem 6:961
13. Liu Z, Wang Y, Chu W, Li Z, Ge C (2010) J Alloys Compd 501:54
14. Ito S, Kuraki J, Tada H, Iwasaki M (1999) J Surface Finish Soc Jpn 50:1171
15. Yerokhin AL, Nie X, Leyland A, Mattews A, Dowey SJ (1999) Surf Coat Technol 122:73
16. Wu CT, Lu FH (2002) Surf Coat Technol 166:31
17. Yerokhin AL, Snizhko LO, Gurevina NL, Leyland A, Pilkington A, Matthew A (2003) J Phys D 36:2110
18. Wu X, Su P, Jiang Z, Meng S (2010) ACS Appl Mater Interfaces 2:808
19. Wan L, Li JF, Feng JY, Sun W, Mao ZQ (2008) Chin J Chem Phys 21:487
20. Yao Z, Jia F, Jiang Y, Li CX, Jiang Z, Bai X (2010) Appl Surf Sci 256:1793
21. Iwasaki M, Iwasaki Y, Tada H, Ito S (2004) Mater Trans 45:1607
22. Kawahara T, Konishi Y, Tada H, Tohge N, Nishii J, Ito S (2002) Angew Chem Int Ed 41:2811
23. Wu X, Wei Q, Zhaohua J (2006) Thin Solid Films 496:288
24. Yao Z, Jia F, Tian S, Li C, Jiang Z, Bai X (2010) ACS Appl Mater Interfaces 2:2617
25. Khomenko VM, Langer K, Rager H, Fett A (1998) Phys Chem Miner 25:338
26. Yen CC, Wang DY, Shih MH, Chang LS, Shih HC (2010) Appl Surf Sci 256:6865
27. Pan L, Zou JJ, Zhang X, Wang L (2010) Ind Eng Chem Res 49:8526
28. Asiltürk M, Sayılkan F, Arpac E (2009) J Photochem Photobiol A 203:64
29. Li H, Liu G, Chen S, Liu Q (2010) Physica E 42:1844
30. Yalçın Y, Kılıç M, Çınar Z (2010) Appl Catal B 99:469
31. West AR (1988) Basic solid state chemistry. Wiley, Chichester
32. Johansson EMJ, Plogmaker S, Walle LE, Schlin R, Borg A, Sandell A, Rensmo H (2010) J Phys Chem C 114:15015
33. Mclntyre NS, Zetaruk DG (1977) Anal Chem 49:1521
34. Sun Z, Yuan H, Liu Z, Han B, Zhang X (2005) Adv Mater 17:2993
35. Konstantinou IK, Albanis TA (2003) Appl Catal B 42:319
36. Ohtani B (2005) Scientific methods in photocatalysis. TokyoT-osho, Tokyo
37. Zuo F, Wang L, Wu T, Zhang Z, Borchardt D, Feng P (2010) J Am Chem Soc 132:11856
38. Ye X, Chen D, Gossage J, Li K (2006) J Photochem Photobiol A 183:35
39. Peng L, Xie T, Lu Y, Fan H, Wang D (2010) Phys Chem Chem Phys 12:8033
40. Tanaka K, Capule MFV, Hisanaga T (1991) Chem Phys Lett 187:73
41. Choi W, Termin A, Hoffmann MR (1994) J Phys Chem 98:13669
42. Zhang W, Li Y, Zhu S, Wang F (2003) J Vac Sci Technol A 21:1877
43. Lu X, Ma Y, Tian B, Zhang J (2011) Solid State Sci 13:625